Electronic Supplementary Material (ESI) for Green Chemistry.

Supplementary Information for

Anodic generation of hydrogen peroxide in continuous flow

Dhananjai Pangotra [a,b], Lénárd-István Csepei [a], Arne Roth [a], Volker Sieber [a,b], Luciana Vieira *[,a]

[a] Fraunhofer Institute of Interfacial Engineering and Biotechnology IGB, Bio-, Electro-, and Chemocatalysis BioCat, Straubing Branch, Schulgasse 11a, 94315, Straubing, Germany

[b] Chair of Chemistry for Biogenic Resources, Campus Straubing for Biotechnology and Sustainability, Technical University of Munich, Schulgasse 16, 94315, Straubing, Germany

List of figures

List of tables

List of schemes

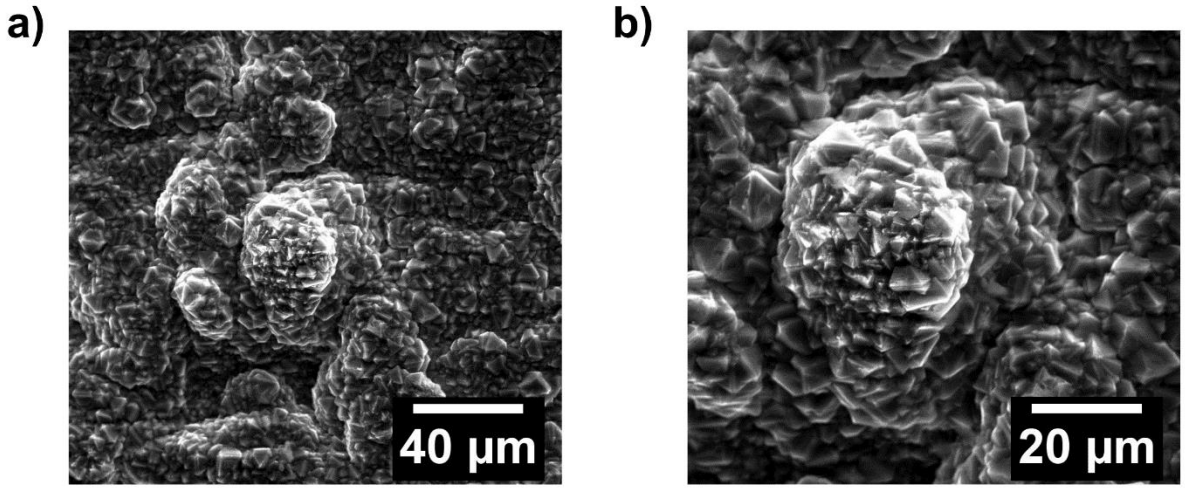

Figure S1 SEM images of used BDD electrode. SEM images of used BDD in this study at different magnification.

The molar fractions for each species were calculated using **Eqs. S2** and **S3**. The experiments were done in highly concentrated electrolytes, which differ from the ideal behavior of diluted electrolytes. As a result, the ion activities ($a_{HCO_3^-}$ and $a_{CO_3^{2-}}$) were calculated as shown in **Eqs. S4** and **S5** using the activity coefficient ($f_\pm$) shown in **Eq. S6**, where z_i is the charge of the ion, A is the Debye-Hückel parameter (0.51 $kg^{½}\ mol^{-½}$, for water at 25 °C), and B is a temperature-dependent parameter. In response to pH changes and carbonate equilibrium, we calculated the activity of HCO_3^- ($a(HCO_3^-)$) and CO_3^{2-} ($a(CO_3^{2-})$) ions during electrolysis for each concentration (c) of $KHCO_3$.

$$K_{a,i} = 10^{-pK_{a,i}} \tag{S1}$$

$$\alpha_{HCO_3^-} = \frac{K_{a,1}.[H^+]}{[H^+]^2 + K_{a,1}.[H^+] + K_{a,1}.K_{a,2}} \tag{S2}$$

$$\alpha_{CO_3^{2-}} = \frac{K_{a,1}.K_{a,2}}{[H^+]^2 + K_{a,1}.[H^+] + K_{a,1}*K_{a,2}} \tag{S3}$$

$$a_{HCO_3^-} = \alpha_{HCO_3^-}.c_{KHCO_3}.f_\pm \tag{S4}$$

$$a_{CO_3^{2-}} = \alpha_{CO_3^{2-}}.c_{KHCO_3}.f_\pm \tag{S5}$$

$$\log f_\pm = -\frac{A.z_i^2.\sqrt{j}}{1+B.a_i.\sqrt{j}} \tag{S6}$$

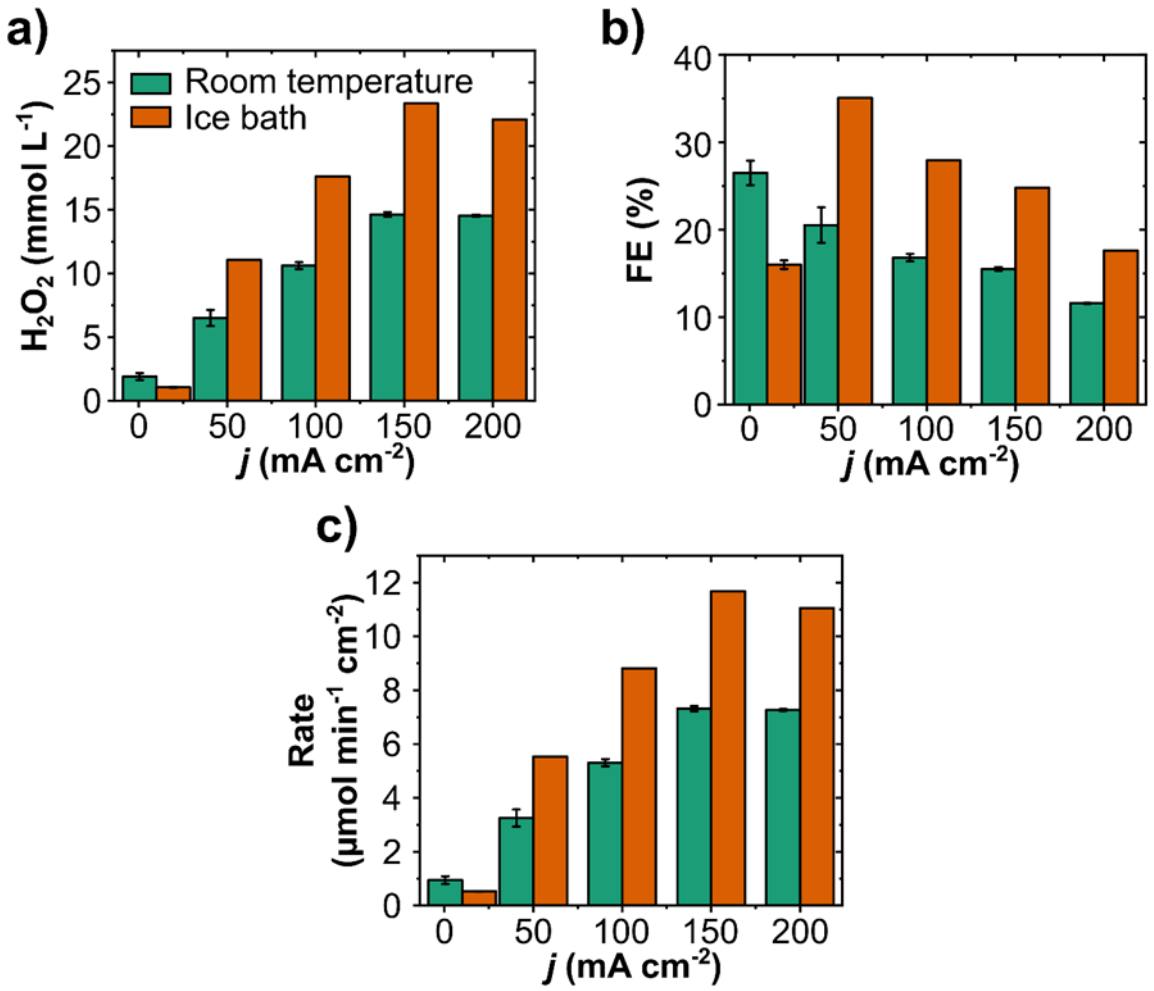

Figure S2 Comparison of electrolyte conditions using BDD as anode. Anodic H_2O_2 **(a)** concentration **(b)** FE, and **(c)** production rate for H_2O_2 production against applied current density during 10 minutes in 25 mL 2 mol L^{-1} $KHCO_3$ (pH 9) at room temperature and in ice bath using 5 cm^2 BDD as an anode in a two compartment H-cell.

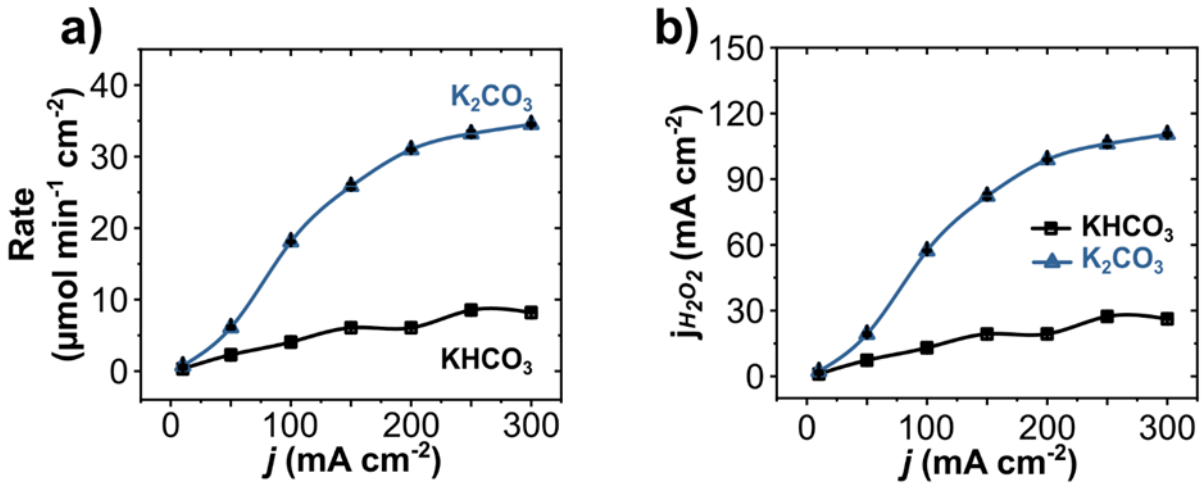

Figure S3 Comparison of electrolyte conditions using BDD as anode. Anodic H_2O_2 **(a)** production rate and **(b)** partial current density for H_2O_2 production against applied current density during 10 minutes in (■) 2 mol L^{-1} $KHCO_3$ at pH 8.4, and (▲) 2 mol L^{-1} K_2CO_3 at pH 12.6 on 5 cm^2 BDD as an anode.

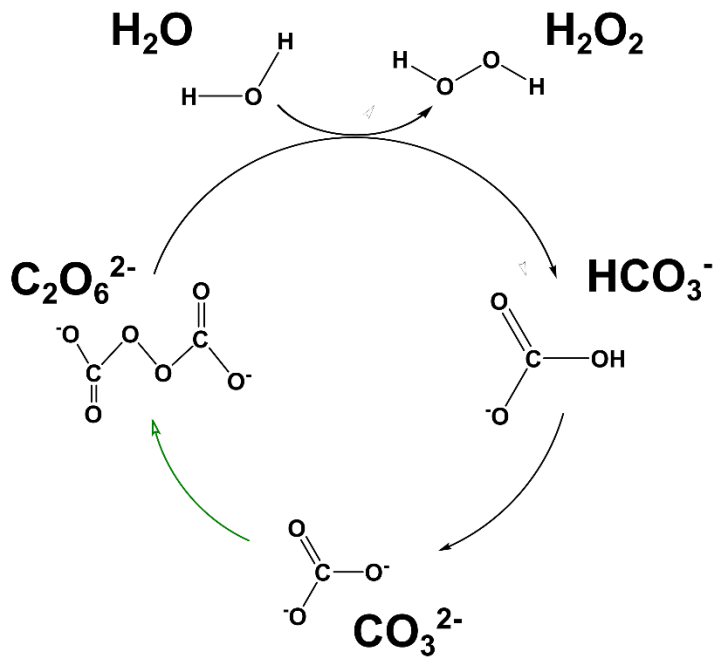

Scheme S1 Scheme for anodic H_2O_2 production in carbonate electrolyte. Carbonate (CO_3^{2-}) can be anodically oxidized to peroxodicarbonate ($C_2O_6^{2-}$) species. $C_2O_6^{2-}$ undergoes hydrolysis to form bicarbonate (HCO_3^-) and hydrogen peroxide (H_2O_2). In alkaline electrolytes, HCO_3^- ions are deprotonated to CO_3^{2-}, which closes the cycle with a higher concentration of H_2O_2.[1]

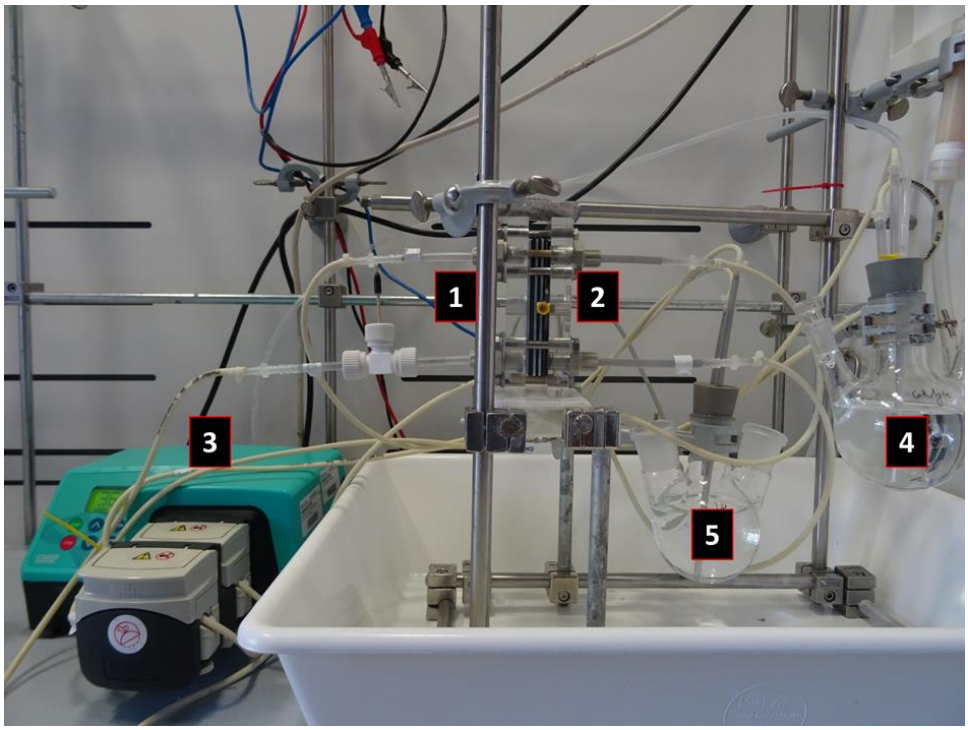

Figure S4 Experimental setup for circular flow. (1) Cathodic compartment, **(2)** anodic compartment, **(3)** flow pump, **(4)** catholyte tank, and **(5)** anolyte tank. The anolyte collected in **(5)** is recirculated to the anodic half-cell and the product is collected in the same reservoir.

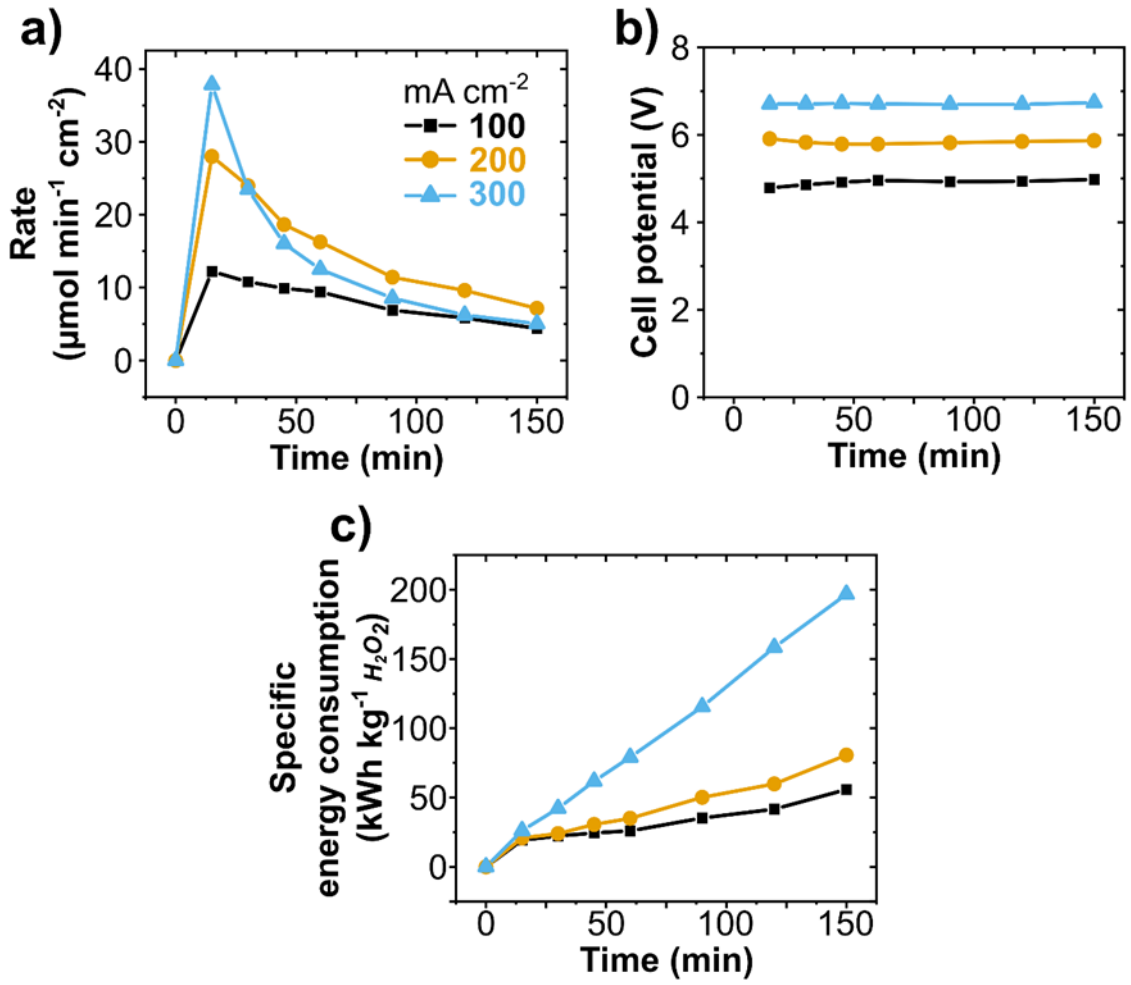

Figure S5 Anodic H_2O_2 production in a circular flow reactor. Anodic H_2O_2 **(a)** production rate, **(b)** cell potential, and **(c)** specific energy consumption to produce 1 kg of H_2O_2 at different current densities using a circular flow system.

Table S1 Anodic H_2O_2 production in a circular flow reactor. Faradaic efficiency and corresponding specific energy consumption to produce 1 kg of H_2O_2 over time at different current densities using a circular flow system.

Time (min)	Faradaic efficiency (%)			Specific energy consumption (kWh^{-1} kg^{-1})		
	100 mA cm^{-2}	*200 mA cm^{-2}*	*300 mA cm^{-2}*	*100 mA cm^{-2}*	*200 mA cm^{-2}*	*300 mA cm^{-2}*
15	39.09	44.86	40.41	0.58	0.62	0.79
30	34.55	38.42	25.08	0.67	0.72	1.27
45	31.72	29.91	17.13	0.73	0.92	1.86
60	30.13	26.09	13.37	0.78	1.05	2.37
90	22.07	18.31	9.14	1.06	1.50	3.47
120	18.70	15.41	6.67	1.25	1.80	4.75
150	14.08	11.48	5.40	1.67	2.42	5.90

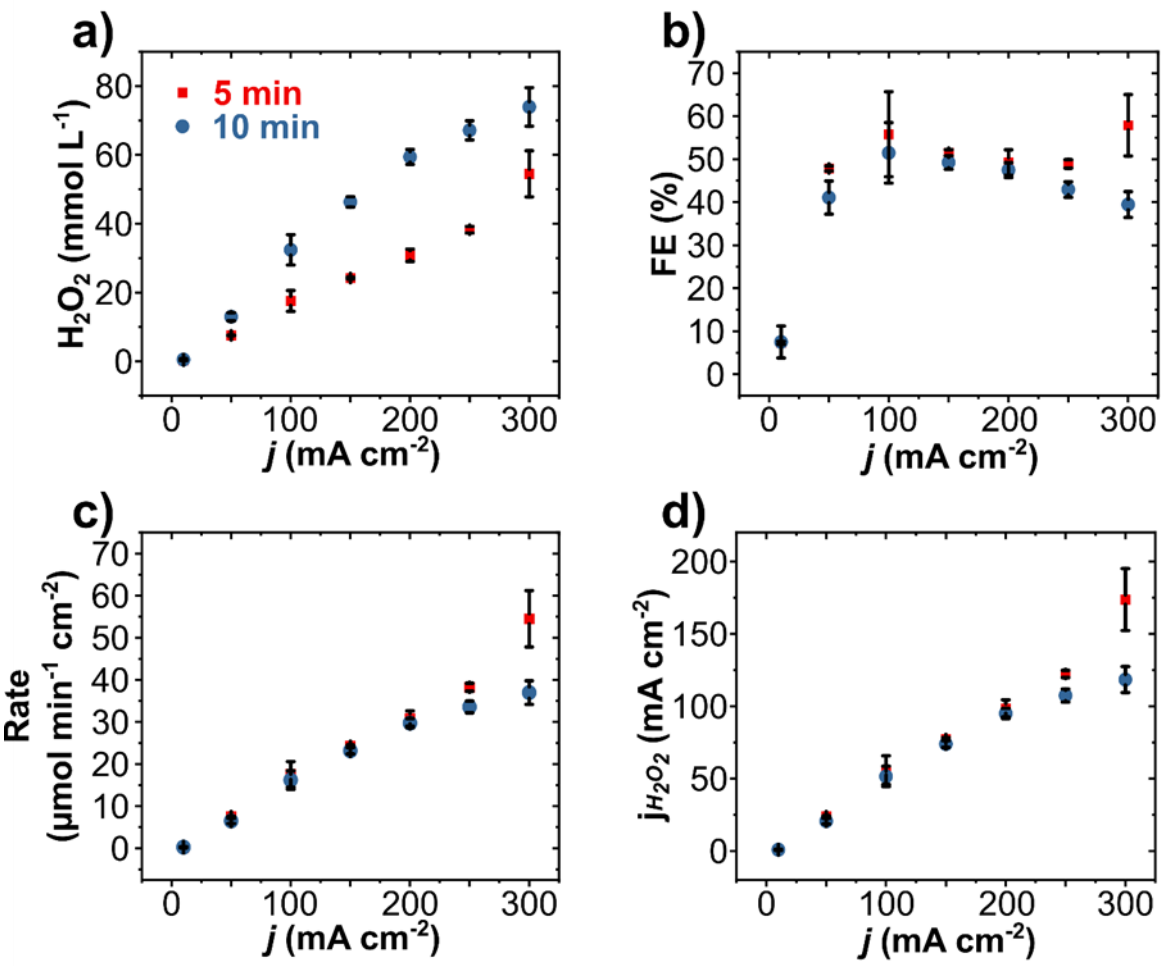

Figure S6 Comparison of the sampling time during electrolysis in H-Cell. (a) Anodic H_2O_2 concentration, **(b)** FE, **(c)** production rate, and **(d)** partial current density at different applied current densities for 5 or 10 minutes. The electrolyte was 2 mol L^{-1} K_2CO_3 at pH 12.6 and the anode a 5 cm^2 BDD.

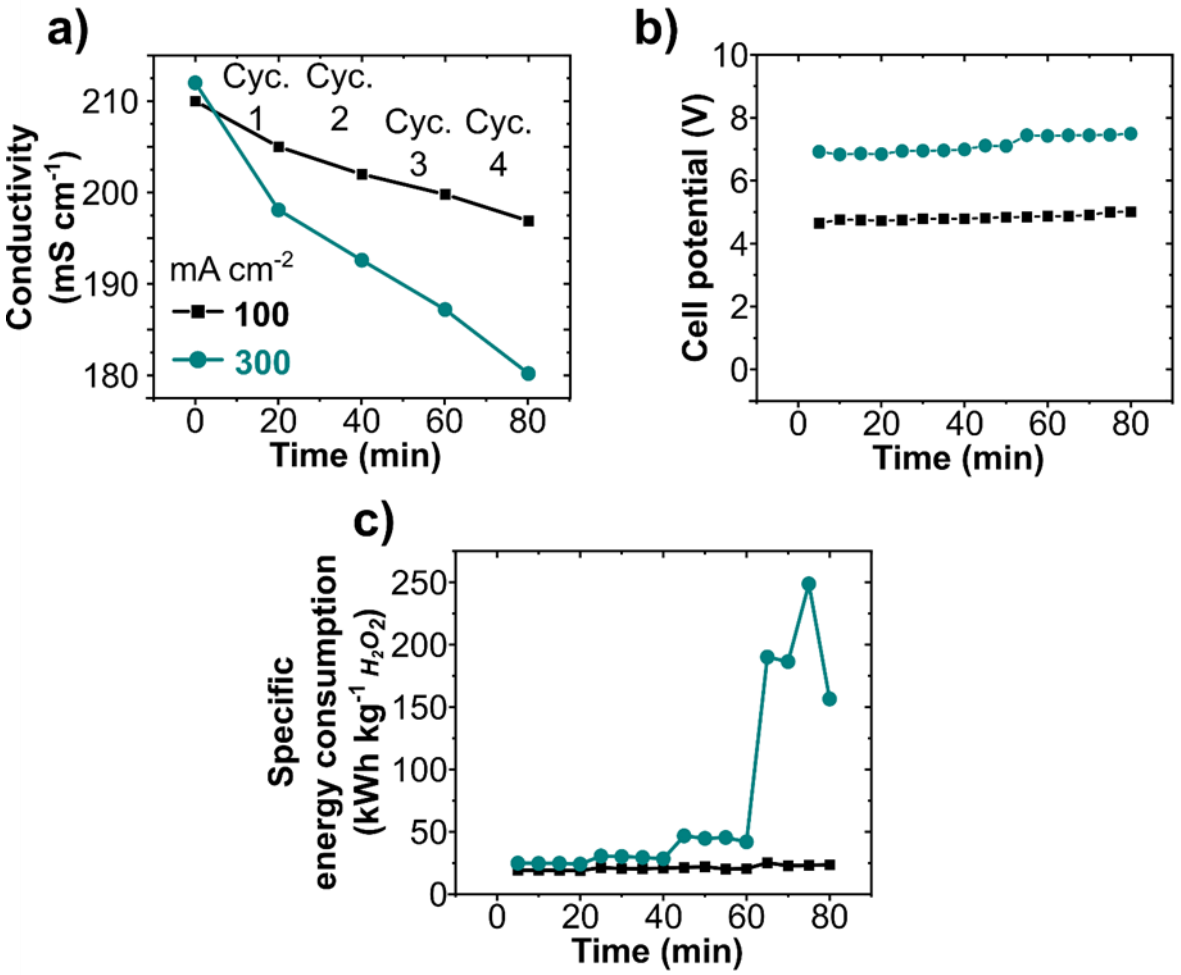

Figure S7 H_2O_2 generation with multiple electrolyte flow cycles. Change in **(a)** conductivity of the electrolyte, **(b)** cell potential, and **(c)** energy consumption against time at a current density of 100 and 300 mA cm^{-2} in 2 mol L^{-1} K_2CO_3 with 90 mmol L^{-1} Na_2SiO_3 stabilizer using 10 cm^2 BDD as an anode. The total volume of the electrolyte used for each cycle was 200 mL. Experiments were performed in a single flow system. The volume accumulated in each cycle was reused in the following one.

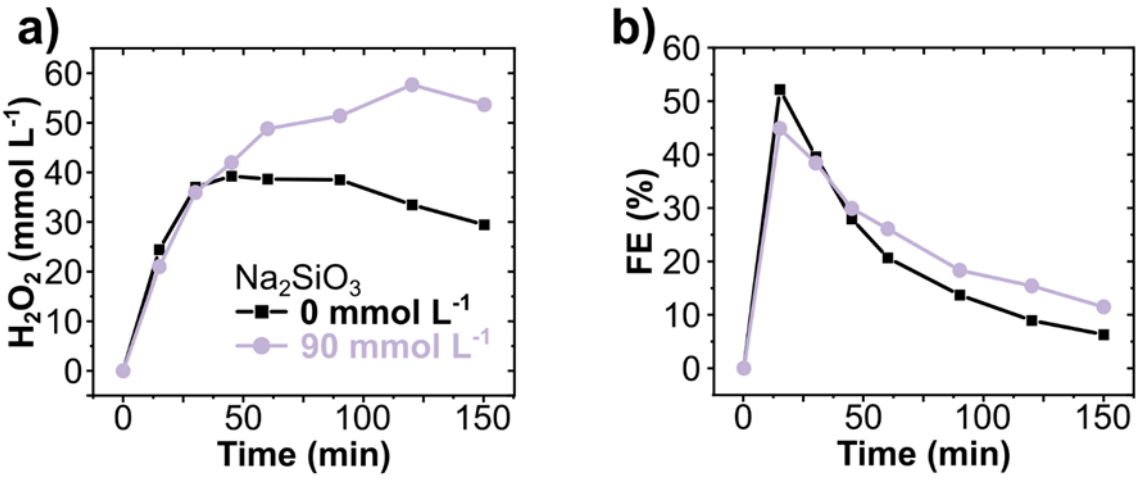

Figure S8 Effect of Na_2SiO_3 stabilizer on H_2O_2 generation in circular flow. Anodic H_2O_2 **(a)** concentration and **(b)** FE at current density of 200 mA cm^{-2} with (■) and without (●) 90 mmol L^{-1} Na_2SiO_3 at a controlled pH of 12.6. Each cell compartment contained a reservoir with 200 mL of 2 mol L^{-1} K_2CO_3 electrolyte circulating at 100 mL min^{-1} flow rate.

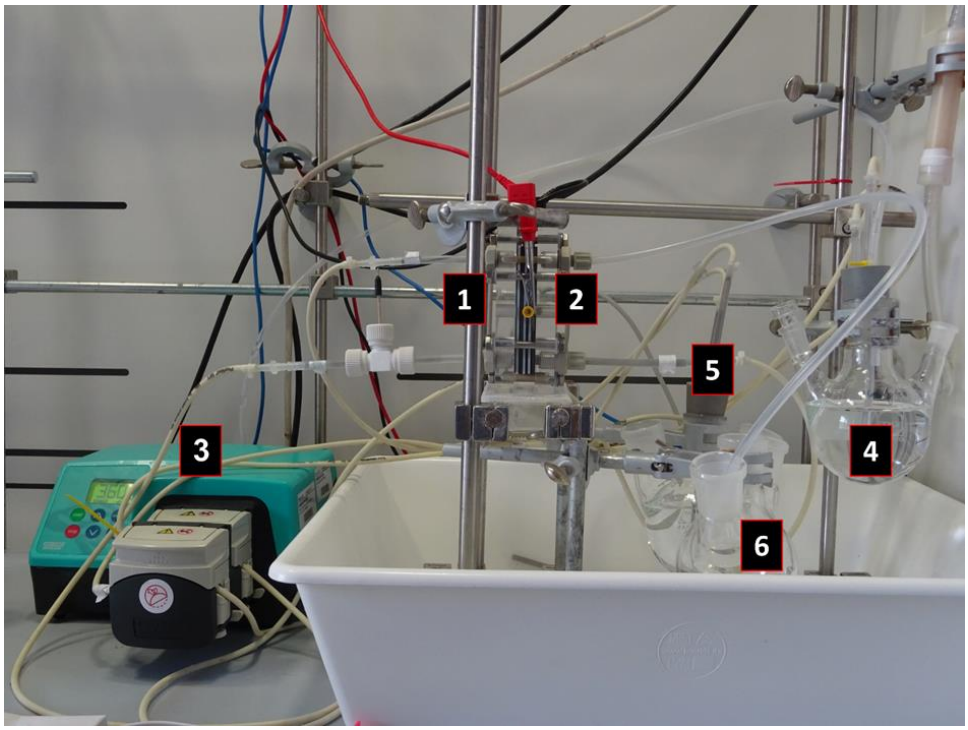

Figure S9 Experimental setup of single-pass flow. (1) Cathodic compartment**, (2)** anodic compartment, **(3)** flow pump, **(4)** catholyte tank, **(5)** fresh anolyte tank before cell, and **(6)** collected anolyte containing H_2O_2 after flow cell.

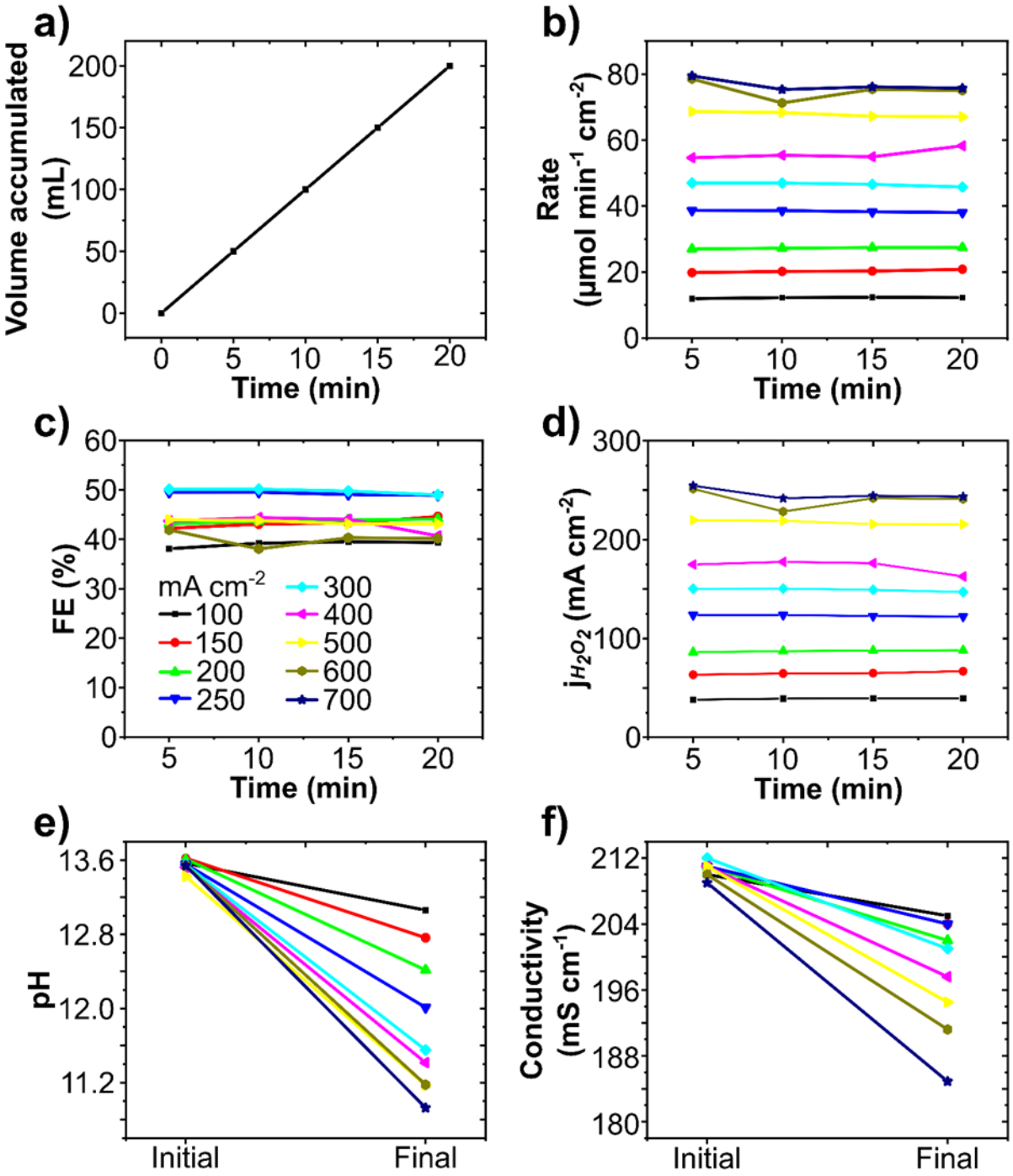

Figure S10 Anodic H_2O_2 production in a single pass mode flow reactor. **(a)** Volume of electrolyte passed over time using a flow rate of 10 mL min^{-1}. **(b)** H_2O_2 concentration, **(c)** FE, and **(d)** current density towards H_2O_2 during 20 min of electrolysis. Change in **(e)** pH and **(f)** conductivity of the electrolyte at different current density in 2 mol L^{-1} K_2CO_3 + 90 mmol L^{-1} Na_2SiO_3. Initial and final pH and conductivity corresponds to 0 and 20 minutes.

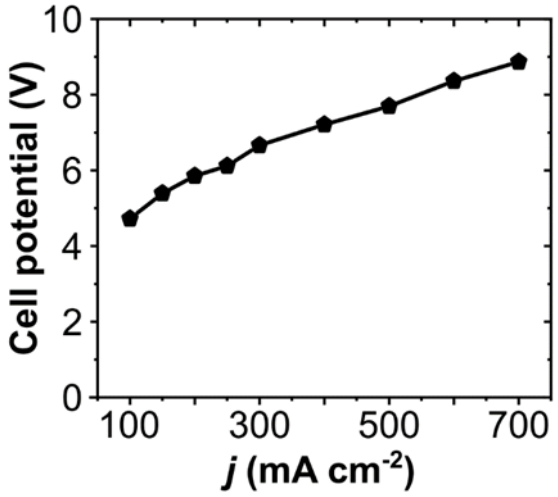

Figure S11 Anodic H_2O_2 production in a single pass mode flow reactor. Cell potential at different current densities using 10 mL min^{-1} flow rate without recirculation in 2 mol L^{-1} K_2CO_3 + 90 mmol L^{-1} Na_2SiO_3.

Table S2 A comparison of the reported work on water oxidation to H_2O_2 with our present study.

Electrode	Cell type	Electro-lyte	Conditions*						$[H_2O_2]_{max}$	Production rate	Peak FE	Ref.
			pH	*j*/P	t	EA	VA	S	*mmol L^{-1}*	*µmol min^{-1} cm^{-2}*	*%*	
PTFE/CFP	H-Cell	1 M Na_2CO_3	12	100	420	0.36	25	~30	3	23.4	66	[2]
BDD/Nb			11.9	39.8	10	1.13	8.5	-	-	3.93	31.7	[3]
BDD/Ti		2 M $KHCO_3$	8	120	5	7.4	25	-	~ 16	~ 8	28	[4]
BDD/Ti			8	295	5	7.4	25	-	29	19.7	~ 22	[4]
$CaSnO_3$@CF-2			~8.3	2.9 V	10	1.3	-	-	-	39.8	90	[5]
$CaSnO_3$/FTO	Undivided		8.3	3.2 V	10	-	30	-	-	~ 4.6	76	[6]
$CaSnO_3$/FTO			8.3	2.2 V	720	-	30	-	~ 0.9	-	-	[6]
$BiVO_4$/FTO		1 M $NaHCO_3$	8.3	3.1 V	-	1	20	-	-	5.7	70	[7]
BDD/Nb	H-Cell	2 M Hybrid	10	300	5	~7	25	-	104.6	76.4	82	[8]
BDD/Nb		5 M K_2CO_3	>13	100	5	~6	25	-	39	15.6	91.5	[9]
CFP	Flow-Cell	2 M K_2CO_3	12.6	100	150	10	200	90	33	4.5	14.3	[1]
BDD/Ta				300	40	10	200	90	76	73	78	This work
				300	80	10	200	90	**110**	46	50	
				700	20	10	200	90	80	**79**	35	

**j: Current density (mA cm^{-2}), P: Potential applied (V vs. RHE), t: Time (minutes), EA: Electrode geometric area (cm^2), VA: Volume of anolyte (mL), S: Stabilizer concentration (mmol L^{-1} Na_2SiO_3)*

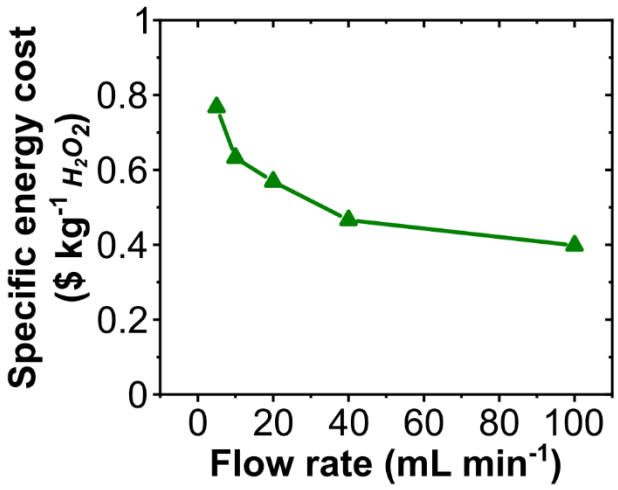

Figure S12 Anodic H_2O_2 generation at different electrolyte flow rates. Specific electricity cost based on energy consumption to produce 1 kg of H_2O_2 at different flow rates. Experiment conditions: Flow cell with 200 mL anolyte at a constant current density (*j*) of 300 mA cm^{-2}.

References

1. D. Pangotra, L.-I. Csepei, A. Roth, C. Ponce de León, V. Sieber and L. Vieira, *Appl. Catal. B Environ.*, 2022, **303**, 120848.
2. C. Xia, S. Back, S. Ringe, K. Jiang, F. Chen, X. Sun, S. Siahrostami, K. Chan and H. Wang, *Nat. Catal.*, 2020, **3**, 125-134.
3. K. Wenderich, B. A. M. Nieuweweme, G. Mul and B. T. Mei, *ACS Sustain. Chem. Eng.*, 2021, **9**, 7803-7812.
4. S. Mavrikis, M. Göltz, S. Rosiwal, L. Wang and C. Ponce de León, *ACS Appl. Energy Mater.*, 2020, **3**, 3169-3173.
5. C. Zhang, R. Lu, C. Liu, L. Yuan, J. Wang, Y. Zhao and C. Yu, *Adv. Funct. Mater.*, 2021, **31**, 2100099.
6. S. Y. Park, H. Abroshan, X. Shi, H. S. Jung, S. Siahrostami and X. Zheng, *ACS Energy Lett.*, 2019, **4**, 352-357.
7. X. Shi, S. Siahrostami, G. L. Li, Y. Zhang, P. Chakthranont, F. Studt, T. F. Jaramillo, X. Zheng and J. K. Norskov, *Nat. Commun.*, 2017, **8**, 701.
8. S. Mavrikis, M. Göltz, S. C. Perry, F. Bogdan, P. K. Leung, S. Rosiwal, L. Wang and C. Ponce de León, *ACS Energy Lett.*, 2021, 2369-2377.
9. S. Mavrikis, M. Göltz, S. Rosiwal, L. Wang and C. Ponce de León, *ChemSusChem*, 2022, **15**, e202102137.